Eur. Phys. J. B **40**, 3–9 (2004)
DOI: 10.1140/epjb/e2004-00232-8

THE EUROPEAN PHYSICAL JOURNAL B

Temperature dependence of the critical current density in proton irradiated YBCO films by magneto-optical analysis

L. Gozzelino[1], D. Botta[1], R. Cherubini[2], A. Chiodoni[1], R. Gerbaldo[1], G. Ghigo[1], F. Laviano[1], B. Minetti[1], and E. Mezzetti[1,a]

[1] Dept. of Physics, Politecnico di Torino and INFM – UdR Torino Politecnico and INFN – Sezione di Torino; C.so Duca degli Abruzzi 24, 10129 Torino, Italy
[2] INFN – Laboratori Nazionali di Legnaro; V.le dell'Università 2, 35020 Legnaro (PD), Italy

Received 10 February 2004 / Received in final form 5 May 2004
Published online 3 August 2004

Abstract. In this paper we present a magneto-optical analysis of local current densities in YBCO films, before and after 3.5 MeV proton irradiation. The main issue consists into measuring and interpreting the temperature dependence of the critical current density (J_c) in samples with different, increasing defect density. Proton irradiation adds more point defects into the as-grown films. The new defect density as well as the related strain-induced modifications of the order parameter are pushed in our experiment up to temperature-modulated damage thresholds. First of all model-independent J_c data were analysed in the framework of different pinning models, all of them based on mechanisms related to the temperature induced change of the effective pinning centre distribution as well as to the shape of single pinning wells. It turns out that in such a framework the fit parameters are, generally speaking, not suitable to interpret the changes of the pinning landscape across the whole investigated temperature range. Then a model based on a vortex distribution across the whole sample, resulting in a current density that mirrors the current through a defect-modulated average short Josephson junction (JJ) row, is successfully tried. The J_c dependence in the whole temperature range and for all the considered defect densities is accounted for by means of a coherent set of fit parameters. It turns out that the chief quantity that allows applying the JJ formalism to a vortex distribution across the defected matrix is a suitably defined temperature-dependent magnetic thickness of the junctions, which substitutes the usual magnetic penetration in JJs.

PACS. 74.25.Sv Critical currents – 61.80.Jh Ion radiation effects – 78.20.Ls Magnetooptical effects – 07.05.Pj Image processing

1 Introduction

High temperature superconducting $YBa_2Cu_3O_{7-\delta}$ (YBCO, henceforth) films are characterized by critical current density (J_c) values orders of magnitude higher than in single crystals. This property is generally investigated in the framework of vortex pinning by different lattice defects, some of them specific for films [1–8]. However, the huge variety of defects [3] claims a phenomenological preview of the film behaviour to be validated in a range of temperature and defect-density as large as possible. This issue is relevant with respect to an extensive use of YBCO as a matrix for micro- and nano-devices. While the magnetic field dependence of J_c has been widely discussed with different approaches [9–12], for what concerns the scenario related to the temperature (T) dependence, no exhaustive description has been reached yet.

Several kinds of pinning mechanism were suggested to explain the J_c dependence on temperature. For example Griessen et al. [13] ascribed temperature dependence of their YBCO films to a spatial variation in the charge-carrier mean free path l near lattice defects (δl-pinning), while Van der Beek et al. [11] suggested that the main pinning centers are extended defects such as sparse second-phase inclusions rather than microscopic point defects. An alternative model was suggested by Klassen et al. [3] who related the high J_c values inside YBCO films mainly to the presence of as-grown linear defects.

With a different approach, Darhmaoui et al. [14] and Yan et al. [15], modelled the film as a bidimensional network of Josephson junctions (JJs) connecting nanoscale domains in the ab planes of YBCO. The authors fitted their J_c vs. T curves with a suitably modified Ambegaokar-Baratoff formula [16]. With a similar

[a] e-mail: enrica.mezzetti@polito.it

approach Jooss et al. [17] found that the anti-phase boundary defects presented in their film behave, for what concerns the temperature dependence of the critical current crossing them, as a high-J_c Josephson junction network. Bernstein et al. [18] ascribed the major role in the transport property control of their YBCO epitaxial films to twin boundaries. In their model such defect-modulated twin boundaries behave as a JJ network.

In previous papers we presented an alternative model [12,19], also based on a junction–like formalism. In the framework of this model the experimental trend found for the critical current in field and temperature was the same that should be observed through an average 1-dimensional row of short, high J_c Josephson junctions. The "hidden" JJ patterns mimicked structural nano-domain patterns, whose dimension was inferred by X-ray diffraction analysis [19].

In this paper we investigate the temperature dependence of J_c at low magnetic fields in thin YBCO films grown by pulsed laser deposition (PLD). The characterizations were performed by means of the quantitative magneto-optical technique, which allows calculating the J_c values without any a priori critical state model assumption or dissipation threshold criteria. The samples were analysed both before and after 3.5 MeV protons irradiation at three different doses. The main analysis was performed by suitably modifying the JJ approach of reference [19], in order to have a self-consistent interpretation of the temperature dependence.

After a short discussion about the J_c dependence on the irradiation dose, we focus on the J_c behaviour as a function of temperature. As a first attempt we fitted our curves before and after irradiation with the standard pinning models quoted in references [3,11,13], trying, without any satisfying outcome, to find single sets of parameters suitable to fit experimental data across the whole temperature range. Afterwards we fitted our experimental data by means of the above-quoted modified Josephson junction formalism. It turns out that in this framework the curves can be easily fitted at any dose by means of coherent sets of parameter values across the whole investigated temperature range.

The paper is organized as follows. The experimental details are reported in Section 2. The experimental data and the analysis in the framework of various pinning models are presented in Section 3.1. Our model and related fit-results are accounted for in Section 3.2. In Section 4 main issues and conclusions are summarized.

2 Experimental details

The analysis was performed on two square-shaped YBCO films, obtained by PLD on (100)-oriented $LaAlO_3$ substrate. The samples were patterned as squares with side about 1 mm long by conventional photolithography and chemical etching. The films are c-axis oriented, with the c-axis perpendicular to the film plane. The first film (labelled #J2_2) is 200 nm thick, while the second one (labelled #J2_4) is 250 nm thick. The superconducting transition temperature of the as-grown films is $T_c = 87.5$ K.

The films were irradiated with 3.5 MeV protons at room temperature and in vacuum at the CN Van der Graff accelerator of the INFN-Laboratori Nazionali di Legnaro (Legnaro, Italy). The beam was directed perpendicular to the film surface. During all the irradiations the particle flux was kept constant at a value lower than 2×10^{11} p/(cm^2 s) (corresponding in our beam geometry to a current lower than 10 nA) in order to avoid local heating. Moreover the samples were mounted on a metallic sample-holder to promote heat dispersion and minimize temperature gradients. The temperature of the sample-holder was checked all along the run by means of a thermocouple. Sample #J2_2 was irradiated at a dose $\phi = 2.5\times10^{15}$ protons/cm^2, while sample #J2_4 was irradiated at a fluence $\phi = 5.0\times10^{15}$ p/cm^2, characterized and then irradiated again up to a total dose $\phi = 1.0\times10^{16}$ p/cm^2. Proton-induced defects consist mostly in point-like defects which, in absence of pre-existing defects, can migrate during irradiation to form clusters [20] and, in a smaller amount, in cascade defects [21,22]. On the contrary, the presence of pre-existing defects acts as "sink" for migrating point-defects [20].

A T_c decrease of about 1 K was measured after the irradiation at the highest dose: it must be reminded that the introduction of microscopic scattering defects by radiation-induced displaced atom, changes the density of state at the Fermi energy, thereby causing a uniform depression of T_c [23]. No change was observed for the other fluences.

The pattern of magnetic flux penetration was visualized using magneto-optical imaging based on the Faraday effect in ferrite garnet indicator films. A description of our experimental set-up can be found elsewhere [24,25]. Magneto-optical images were converted to magnetic induction field maps, $B_z(x,y)$, by means of a suitable non-linear calibration curve obtained in a zone of the indicator film far enough from the sample, in order not to detect the magnetic field induced by the sample itself [24,25]. The local current density (J) values were calculated from the $B_z(x,y)$ maps (Fig. 1a) using inversion of the Biot-Savart law (Fig. 1b) [25,26], with the assumption that the current distribution is parallel to the sample surface and averaged over the sample thickness [25,27]. In the vortex penetrated part of the sample the current density is almost independent of the position on the film surface (Fig. 1c, d). J_c was obtained from the J values in the plateau region of the J vs. position curve and defined as the current density where the maximum pinning sets up. The J_c dependence on local magnetic field exhibits a Bean-like behaviour [25,28].

All magneto-optical characterizations were performed in zero-field cooling, at temperatures ranging from 5 K to 70 K. After each cooling down to the planned temperature a sequence of increasing magnetic field was applied. Each magneto-optical image was acquired 3 s after each field set up.

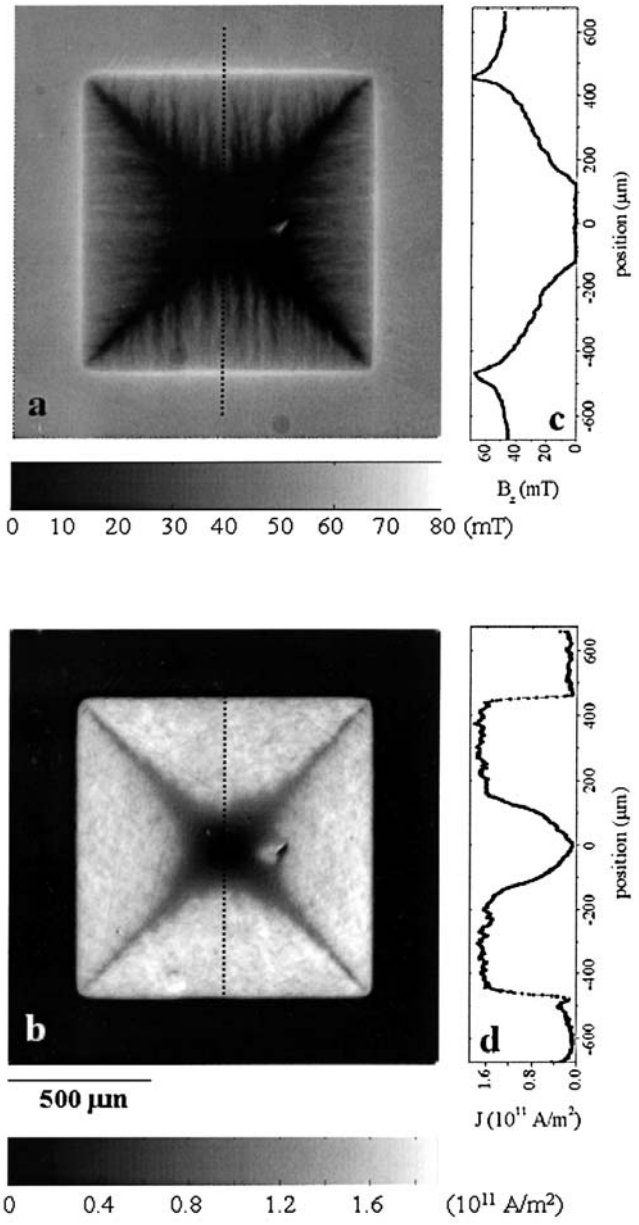

Fig. 1. (a) B_z map and (b) corresponding J map obtained by a magneto-optical image of the sample #J2_4 before irradiation at $T = 5$ K and $\mu_0 H_{ext} = 43.3$ mT. In (c) and (d) the B_z and J profiles evaluated along the dotted lines of Figures (a) and (b) are plotted, respectively.

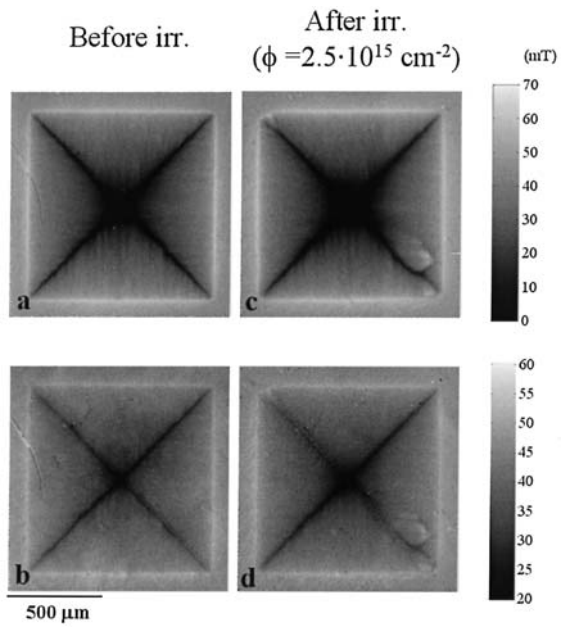

Fig. 2. Sample #J2_2 – Magnetic field penetration maps obtained before and after irradiation at $T = 15$ K (top) and $T = 55$ K (bottom). External applied field: $\mu_0 H_{ext} = 43.3$ mT.

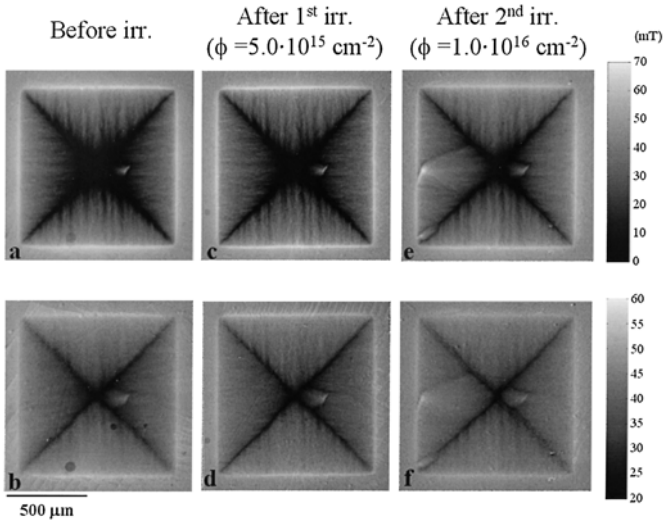

Fig. 3. Sample #J2_4 – Magnetic field penetration maps obtained before and after the two irradiation doses at $T = 15$ K (top) and $T = 55$ K (bottom). External applied field: $\mu_0 H_{ext} = 43.3$ mT.

3 Experimental results and discussion

3.1 Experimental results and analysis with pinning models

In Figures 2 and 3 magnetic induction penetration maps of the samples #J2_2 and #J2_4 are plotted before and after irradiation at $T = 15$ K (Figs. 2a, c, Figs. 3a, c, e) and at 55 K (Figs. 2b, d, Figs. 3b, d, f). All the reported images were taken in an external applied field $\mu_0 H_{ext} = 43.3$ mT. This external field indeed results to be representative of the irradiation effect on the penetration pattern in the low magnetic field range investigated ($0 \div 150$ mT). Magnetic flux penetrates the films following the geometrical constraints imposed by the square shape [29]. The discontinuity lines along the diagonals, where the current stream lines bend, do not show "as-grown" or irradiation-induced anisotropy [30] (unless in the case of alteration of the flux line penetration due to more or less extended, casual scratches).

At the lowest fluence ($\phi = 2.5 \times 10^{15}$ p/cm^2 – Fig. 2) the film is less penetrated than before irradiation and the corresponding J_c enhancement is about 15% in the

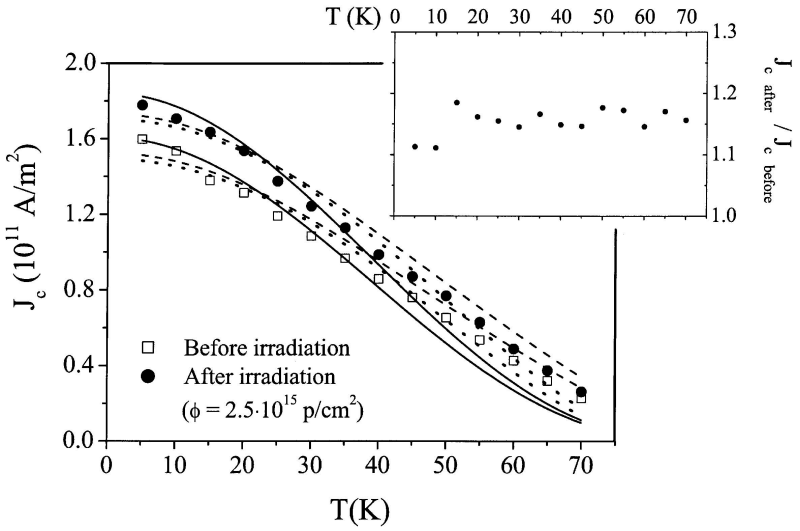

Fig. 4. Sample #J2_2 – Experimental critical current density dependence on temperature (symbols) evaluated before and after irradiation in correspondence to a local magnetic induction field of 20 mT. In the inset the ratio of the J_c values measured after and before irradiation is plotted. The lines in the main figure are the best fitting curves of the experimental data with the formulas predicted i) by the 3-dimensional δl-pinning model described in reference [13] (solid lines), ii) by a pinning mechanism accounting for an as-grown linear defect distribution described in reference [3] (dotted lines), iii) by a pinning mechanism mainly ascribed to extended defects such as sparse second-phase inclusions as in reference [11] (dashed lines).

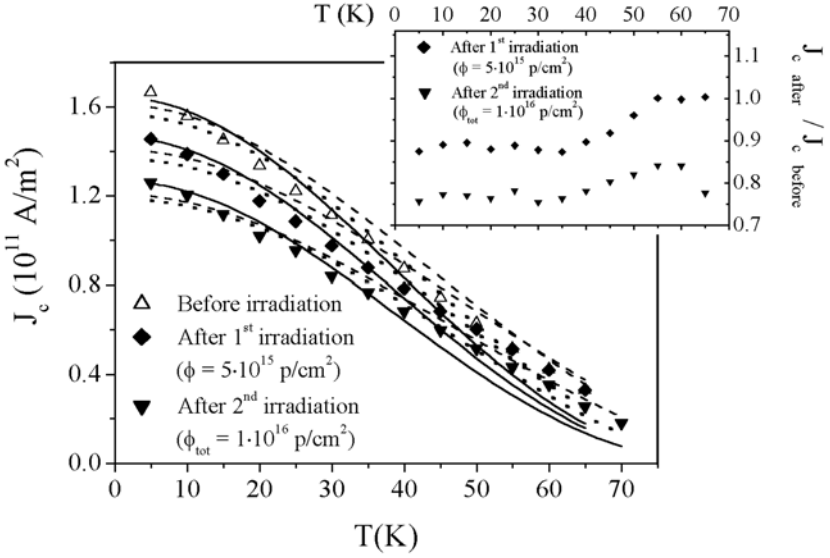

Fig. 5. Sample #J2_4 – Experimental critical current density dependence on temperature (symbols) evaluated before and after each irradiation in correspondence to a local magnetic induction field of 20 mT. In the inset the ratios of the J_c values measured after each irradiation and those measured before irradiation are plotted. The lines in the main figure are the best fitting curves of the experimental data with the formulas predicted i) by the 3-dimensional δl-pinning model described in reference [13] (solid lines), ii) by a pinning mechanism accounting for an as-grown linear defect distribution described in reference [3] (dotted lines), iii) by a pinning mechanism mainly ascribed to extended defects such as sparse second-phase inclusions as in reference [11] (dashed lines).

whole investigated range of temperatures (Fig. 4). With respect to the as-grown film as well as to the enhanced one, at larger fluences ($\phi = 5.0 \times 10^{15}$ p/cm^2 and $\phi = 1.0 \times 10^{16}$ p/cm^2) the field maps exhibit a wider field penetration at low temperatures (Figs. 3c, e) while at higher temperatures, a complete (after irradiation at $\phi = 5.0 \times 10^{15}$ p/cm^2, Fig. 3d) or a partial (after the irradiation at $\phi = 1.0 \times 10^{16}$ p/cm^2, Fig. 3f) J_c recovering are exhibited. The trends are summarized in Figure 5. The crossover enhancement-damage with increasing proton dose is expected because at higher doses the active flow area is strongly reduced [31].

First of all we tried to fit our experimental curves with models based on the temperature dependence of pinning

wells in a contest of outstanding pinning models. Following the model suggested by Griessen et al. [13], in the framework of a J_c vs. T behaviour predicted by a 3-dimensional δl-pinning mechanism, it was possible to find an optimal parameter set only for the low temperature data. On the other hand following the model described by Van der Beek et al. [11] or the model suggested by Klassen et al. [3], a satisfying agreement between the fitting and the experimental curves was not also found by using a unique set of parameters for the whole range of temperatures. However, in these last two cases, it was possible to fit the whole curves using different sets of parameters at low and at high temperatures, respectively: namely, parameter ensembles resulting optimal for low temperature data, turned out not to be adequate for temperatures higher than 40 K, or vice versa. Some typical fit behaviours are reported in Figures 4 and 5.

3.2 Junction–like formalism based model and related results

In a different framework we assumed that the vortex lattice arrangement at all temperatures results in a critical current density whose temperature and field behaviour is consistent with that expected by current density crossing an average 1-dimensional network of short Josepshon junctions [19]. It can be visualized as a wall faceted by regions of nanometric size, where the order parameter is heavily changed, situated between two contiguous electrodes [12,19,32]. Each JJ, whose length is determined by the average defect distribution, passes current according to its Fraunhofer pattern [33]. The junctions are characterized by a temperature dependent magnetic thickness (see below) [12,19,34]. Several classes of defects in high temperature superconductors could be responsible for a JJ-like nature of the macroscopic flowing current. More outstandingly, Josephson junction-like effects can be observed even in absence of real junctions, when particular dynamic regimes of the vortex lattice resulting in phase slip lines are established [35–38].

In the present paper we started from the formula of the critical current density, j_{cj}, across a single junction suggested by Cardoso et al. [39]. In a framework of Josephson-based formalisms it allows a self-consistent and clear approach to the problem of the temperature dependence of J_c. The proposed expression of j_{cj} was obtained by defining a suitable junction-induced superconducting decoherence length $\varepsilon = \varepsilon_0(1 - T/T_c)^{-\gamma}$ which affects the temperature dependence of the superconducting order parameter in the junction region. On the other hand, to account for the temperature dependence of the electrodynamical constraints felt by the vortex penetration patterns across the whole defected matrix, we suitably modified the original j_{cj} formula by introducing an explicit temperature and field dependence of the average junction-row magnetic thickness, $\Lambda(B,T)$ [19,34,40]. Such a dependence, as suggested by the scaling behaviour with temperature of the $J_c(B,T)$ curves reported in [19], in presence of vortices in the "junction electrodes" can be expressed by $\Lambda(B,T) = \zeta(T)(\Phi_0/B)^{1/2} = \zeta_0(1 - T/T_c)^{-0.5}(\Phi_0/B)^{1/2}$. The quantity $\Lambda(B,T)$ substitutes the usual JJ magnetic penetration length [33]. Therefore, by introducing the parameter $\eta(T) = \Lambda(\mathrm{T})/\varepsilon_0$, j_{cj} across a single junction can be expressed as [39]:

$$j_{cj}(T) = J_0\,\tau^{\gamma}\left[\frac{1-\tanh(\tau^{\gamma}\eta)}{\cosh^2(\tau^{\gamma}\eta)}\,\frac{\cosh^2(\eta_0)}{1-\tanh(\eta_0)}\right]\frac{\sin\dfrac{\pi\Phi}{\Phi_0}}{\dfrac{\pi\Phi}{\Phi_0}}$$

where $\tau = (1 - T/T_c)$, $\eta_0 = \eta(T = 0)$ and $\Phi = B\Lambda L$ (Φ, effective flux across the junction; L, junction length and B local field value). In summary, the temperature dependence of j_{cj} accounts separately for the temperature dependence of the decoherence length and of the magnetic thickness.

To take into account the statistical distribution of the junction contact lengths, we considered a suitable probability density function $p(L)$. J_0 was supposed to be the same for all the junctions. Therefore the critical current density can be obtained as the average of the j_{cj} values of the single junctions, weighted by $p(L)$. Thus the macroscopic critical current density, J_c, takes the form:

$$J_c = J_0\int_0^{\infty} dL\,p(L)\,\tau^{\gamma}\left(\frac{1-\tanh\tau^{\gamma}\eta}{1-\tanh\eta_0}\right)\Big/\left(\frac{\cosh^2\tau^{\gamma}\eta}{\cosh^2\eta_0}\right) \times\left|\frac{\sin\,(\pi B\Lambda_0 L/\Phi_0)}{\pi B\Lambda_0 L/\Phi_0}\right|. \quad (1)$$

We assumed $p(L) = k^2 L e^{-kL}$ where $k = 2/\langle L\rangle$. By putting $\beta = k\Phi_0\tau^{0.5}/(\pi B\Lambda_0) = \beta_0\tau^{0.5}$, the integral of equation (1) can be solved analytically, so that the macroscopic critical current density can be written as:

$$J_c = J_0\tau^{\gamma}\left(\frac{1-\tanh\tau^{\gamma}\eta}{1-\tanh\eta_0}\right)\Big/\left(\frac{\cosh^2\tau^{\gamma}\eta}{\cosh^2\eta_0}\right) \times\frac{\beta^2/(\beta^2+1)}{\beta_0^2/(\beta_0^2+1)}\,\frac{\coth(\pi\beta/2)}{\coth(\pi\beta_0/2)}. \quad (2)$$

We fitted the experimental J_c values with equation (2). It turns out that the agreement between the experimental data and the fit curves is satisfactory both before and after irradiation (Figs. 6a and 6b). The fitting parameter values J_0, γ, η_0, β_0 are reported in Table 1 for both samples. The data shown in the above quoted figures as well as the relative fitting curves and parameters were evaluated at a given internal local induction field, $B_z = 20$ mT. They can be considered representative of the J_c vs. T behaviour in our samples at low fields. Namely, by the comparison between the Figures 1c and 1d, in the vortex penetrated part of the samples, the current density profile exhibits a constant behaviour despite the change of the local field. Moreover also by changing the external applied field in the range explored with our magneto-optical analysis (up to 150 mT) no significant J_c changes as a function of field are exhibited [28].

Table 1. Fit parameter values obtained by the best fitting of the critical current density dependence on temperature of both the films before and after irradiations with equation (2). In the last row the mean values of the Josephson junction length as deduced by the fits are reported. The reported errors are the diagonal elements of the co-variance matrix evaluated from the second derivatives of the chi-square function [41].

	#J2_2 before irr.	#J2_2 after irr. $\phi = 2.5 \times 10^{15}$ p/cm^{-2}	#J2_4 before irr.	#J2_4 after irr. $\phi = 5.0 \times 10^{15}$ p/cm^{-2}	#J2_4 after irr. $\phi = 1.0 \times 10^{16}$ p/cm^{-2}
J_0 (10^{11} A/m^2)	1.67 ± 0.01	1.89 ± 0.02	1.77 ± 0.01	1.54 ± 0.01	1.34 ± 0.01
γ	1.48 ± 0.02	1.49 ± 0.05	1.44 ± 0.01	1.39 ± 0.04	1.43 ± 0.02
η_0	0.34 ± 0.01	0.36 ± 0.03	0.26 ± 0.01	0.29 ± 0.01	0.31 ± 0.01
β_0	6.70 ± 0.29	7.34 ± 0.30	7.71 ± 0.40	9.71 ± 0.88	12.94 ± 0.94
$\langle L \rangle$(nm)	30.5 ± 1.3	27.9 ± 1.1	26.5 ± 1.4	21.1 ± 1.9	15.8 ± 1.2

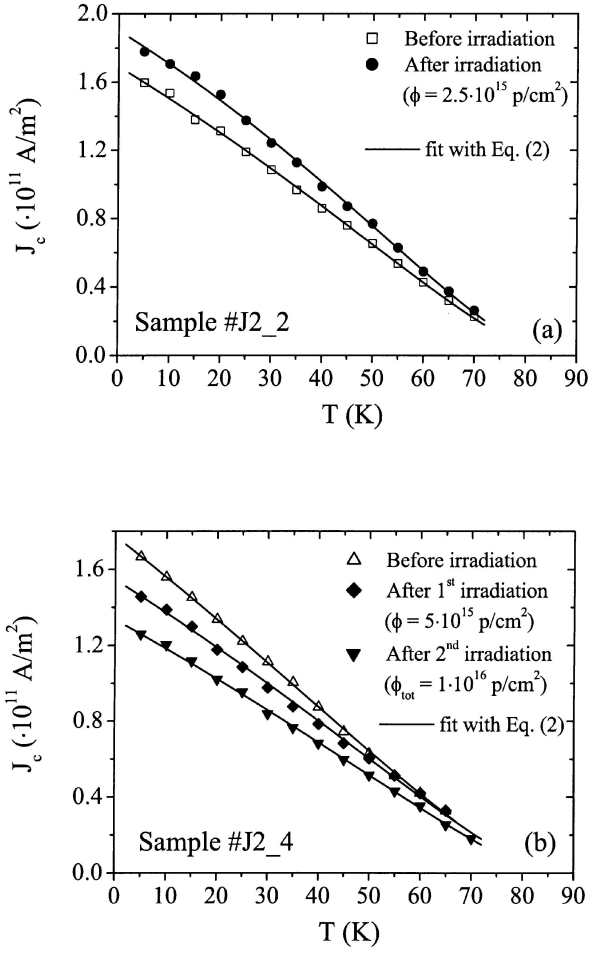

Fig. 6. Experimental critical current density dependence on temperature (symbols) evaluated before and after irradiations for the sample #J2_2 (a) and #J2_4 (b) at a local magnetic induction field of 20 mT and corresponding best fitting curves (solid lines) with the equation (2) (see text).

The increasing of both $\beta_0 = k\Phi_0/(\pi B \Lambda_0)$ and η_0 parameters after irradiation are consistent with the expectation of the chosen model [12,19]. Namely the expression $\Lambda(B,T) = \zeta(T)(\Phi_0/B)^{1/2} = \zeta_0(1 - T/T_c)^{-0.5}(\Phi_0/B)^{1/2}$ for the magnetic thickness is equivalent to the assumption of ζ_0 as a pure geometric parameter. From β_0 values, assuming that $\zeta_0 \approx 1$ [19,34] both before and after irradiation, we can estimate the change of the mean value $\langle L \rangle$ of the junction length distribution. Consistently, $\langle L \rangle$ decreases after irradiation (as reported in the last row of Tab. 1). Moreover, taking into account that the fit parameter η_0 depends on the inverse of the decoherence length, following the model suggested in reference [39], its increase after irradiation can indicate on average an irradiation-induced stronger depression of the superconducting order parameter inside the junction-like pattern.

4 Conclusions

In this paper the effect of the 3.5 MeV proton irradiation on critical current density in *c*-axis oriented YBCO thin films was investigated by means of quantitative magneto-optical analysis. The irradiation fluence was increased up to temperature-modulated damage thresholds. Namely a temperature dependent crossover from enhancement to J_c damage is exhibited by increasing the irradiation doses. In order to gain insights into the mechanisms controlling the collective vortex lattice behaviours limiting the current flow, the J_c dependence on temperature was analysed before and after irradiation, at three different doses. Looking forward to the application of YBCO films for electronic devices with reproducible performances in hard environment, this aspect has to be checked in presence of defect densities lying in a large range of values, and across a wide range of temperature. It turns out that, both before and after irradiation and in the whole analysed temperature range, the J_c vs. T curves can be accounted for by a JJ-like formalism [38]. In particular the vortex lattice arrangement at all temperatures results in a current density mirroring the current across an average row of short Josepshon junctions, whose length is determined by the defect density. The chief quantity that allows applying the JJ formalism to a vortex distribution in a defected matrix is a suitably defined temperature-dependent magnetic thickness of the junctions, which substitutes the usual magnetic penetration in JJs.

In conclusion Josephson junction-like effects could dominate the vortex lattice lay-outs and fast dynamics across heavily defected YBCO films.

Financial support from INFN under Na.St.R.I. experiment is gratefully acknowledged. We also acknowledge the ESF VORTEX programme.

References

1. J. Mannhart, D. Anselmetti, J.G. Bednorz, A. Catana, Ch. Gerber, K.A. Mueller, D.G. Schlomm, Z. Phys. B: Condens. Matter **86**, 177 (1992)
2. H. Douwes, P.H. Kes, Ch. Gerber, J. Mannhart, Cryogenics **33**, 486 (1993)
3. F.C. Klassen, G. Doornbos, J.M. Huijbregtse, R.C.F. van der Geest, B. Dam, R. Greissen, Phys. Rev. B **64**, 184523 (2001)
4. H.W. Weber, R.M. Schalk, K. Kundzins, E. Stangl, S. Proyer, D. Baüerle, Physica C **257**, 341 (1996)
5. D.S. Misra, B.D. Padalia, S.P. Pai, R. Pinto, S.B. Palmer, Thin Solid Films **245**, 186 (1994)
6. T. Haage, J. Zegenhagen, J.Q. Li, H.-U. Habermeier, M. Cardona, Ch. Jooss, R. Warthmann, A. Forkl, H. Kronmüller, Phys. Rev. B **56**, 8404 (1997)
7. H. Kronmüller, Ch. Jooss, A. Forkl, R. Warthmann, H.-U. Habermeier, B. Leibold, Physica C **266**, 235 (1996)
8. Ch. Jooss, A. Forkl, R. Warthmann, H.-U. Habermeier, B. Leibold, H. Kronmüller, Physica C **266**, 235 (1996)
9. J.M. Huijbregtse, B. Dam, R.C.F. van der Geest, F.C. Klassen, R. Elberse, J.H. Rector, R. Griessen, Phys. Rev. B **62**, 1338 (2000)
10. B. Dam, J.M. Huijbregtse, F.C. Klassen, R.C.F. van der Geest, G. Doornbos, J.H. Rector, A.M. Testa, S. Freisem, J.C. Martinez, B. Stäuble-Pümpin, R. Greissen Nature **399**, 439 (1999); B. Dam, J.H. Rector, J.M. Huijbregtse, R. Griessen, Physica C. **305**, 1 (1998)
11. C.J. Van der Beek, M. Konczykowski, A. Abal'oshev, I Abal'osheva, P. Gierlowski, S.J. Lewandowski, M.V. Indenbom, S. Barbanera, Phys. Rev. B **66**, 024523 (2002)
12. E. Mezzetti, R. Gerbaldo, G. Ghigo, L. Gozzelino, B. Minetti, C. Camerlingo, A. Monaco, G. Cuttone, A. Rovelli, Phys. Rev. B **60**, 7623 (1999)
13. R. Griessen, Wen Hai-hu, A.J.J. van Dalen, B. Dam, J. Rector, H.G. Schnack, S. Libbrecht, E. Osquiguil, Y. Bruynseraede, Phys. Rev. Lett. **72**, 1910 (1994); A.J.J. van Dalen, R. Griessen, S. Libbrecht, Y. Bruynseraede, E. Osquiguil, Phys. Rev. B **54**, 1366 (1996)
14. H. Darhmaoui, J. Jung, Phys. Rev. B **53**, 14621 (1996); H. Darhmaoui, J. Jung, Phys. Rev. B **57**, 8009 (1998)
15. H. Yan, J. Jung, H. Darhmaoui, Z.F. Ren, J.H. Wang, W.-K. Kwok, Phys. Rev. B **61**, 11711 (2000)
16. J. Clem, B. Bumble, S.I. Raider, W.J. Gallagher, Y.C. Shih, Phys. Rev. B **35**, 6637 (1987)
17. Ch. Jooss, R. Warthmann, H. Kronmüller, T. Haage, H-U. Habermeier, J. Zegenhagen, Phys. Rev. Lett. **82**, 632 (1999)
18. P. Bernstein, J.F. Hamet, J. Appl. Phys. **95**, 2569 (2004)
19. E. Mezzetti, A. Chiodoni, R. Gerbaldo, G. Ghigo, L. Gozzelino, B. Minetti, C. Camerlingo, C. Giannini, Eur. Phys. J. B **19**, 357 (2001)
20. B.M. Vleck, H.K. Viswanathan, M.C. Frischherz, S. Fleshler, K. Vandervoort, J. Downey, U. Welp, M.A. Kirk, G.W. Crabtree, Phys. Rev. B **48**, 4067 (1993)
21. J.F. Ziegler et al., *The Stopping and Range of Ions in Solids* (Pergamon Press, New York, 1985), Vol. 1
22. M.A. Kirk, Y. Yan, Micron **30**, 507 (1999)
23. Y.J. Zhao, W.K. Chu, M.F. Davis, J.C. Wolfe, S.C. Deshmukh, D.J. Economou, A. Mcguire, Physica C **184**, 144 (1992)
24. L. Gozzelino, A. Chiodoni, R. Gerbaldo, G. Ghigo, F. Laviano, E. Mezzetti, B. Minetti, R. Fastampa, Int. J. Mod. Phys. B **14**, 2866 (2001)
25. F. Laviano, D. Botta, A. Chiodoni, R. Gerbaldo, G. Ghigo, L. Gozzelino, S. Zannella, E. Mezzetti, Supercond. Sci. Technol. **16**, 71 (2003)
26. Ch. Jooss, R. Warthmann, A. Forkl, H. Kronmuller, Physica C **299**, 215 (1998); Ch. Jooss, J. Albrecht, H. Kuhn, S. Leonhardt, H. Kronmuller, Rep. Prog. Phys. **65**, 651 (2002)
27. G.P. Mikitik, E.H. Brandt, Phys. Rev. B **62**, 6800 (2000)
28. F. Laviano, D. Botta, A. Chiodoni, R. Gerbaldo, G. Ghigo, L. Gozzelino, E. Mezzetti, Phys. Rev. B **68**, 014507 (2003)
29. Th. Schuster, M.V. Indenbom, M.R. Koblischka, H. Kuhn, H. Kronmüller, Phys. Rev. B **49**, 3443 (1994)
30. Ch. Jooss, R. Warthmann, H. Kronmüller, Phys. Rev. B **61**, 12433 (2000)
31. A. Gandini, R. Weinstein, D. Parks, R.P. Sawh, S.X. Dou, IEEE Trans. Appl. Supercond. **13**, 2934 (2003) and reference therein
32. A. Gurevich, L.D. Cooley, Phys. Rev. B **50**, 13563 (1994)
33. A. Barone, G. Paternò, *Physics and Applications of the Josephson Effect* (Wiley, New York, 1982)
34. Y. Cai, A. Gurevich, I. Fei-Tsu, D.L. Kaiser, S.E. Babcock, D.C. Larbalestier, Phys. Rev. B **57**, 10591 (1998)
35. K.K. Likharev, Sov. Phys. JEPT **34**, 906 (1972)
36. L.G. Aslamazov, A.I. Larkin, Sov. Phys. JEPT **41**, 381 (1975)
37. Y. Yuzhelevski, G. Jung, C. Camerlingo, M. Russo, M. Ghinovker, B.Ya. Shapiro, Phys. Rev. B **60**, 9726 (1999)
38. A.G. Sivakov, A.M. Glukhov, A.N. Omelyanchouk, Y. Koval, P. Müller, A.V. Ustinov, Phys. Rev. Lett. **91**, 267001 (2003)
39. J.L. Cardoso, P. Pereyra, Phys. Rev. B **61**, 6360 (2000)
40. M.V. Fistul', G.F. Giuliani, Phys. Rev. B **51**, 1090 (1995)
41. A.A. Clifford, *Multivariate error analysis* (Applied Science Publishers LTD, London, 1971)